ACS APPLIED MATERIALS & INTERFACES

www.acsami.org

Research Article

Highly Sensitive and Selective Organic Gas Sensors Based on Nitrided ZSM-5 Zeolite

Yea Eun Hahm,[†] Sungjoon Kweon,[†] Min Bum Park,* and Yeong Don Park*

Cite This: *ACS Appl. Mater. Interfaces* 2023, 15, 7196−7203

Read Online

ACCESS | Metrics & More | Article Recommendations | Supporting Information

ABSTRACT: For next-generation gas sensors, conductive polymers have strong potential for overcoming the existing deficiencies of conventional inorganic sensors based on metallic oxides. However, the signal of organic gas sensors is inferior to that of inorganic metal oxide gas sensors because of organic gas sensors' poor charge carrier transport. Herein, the combination of an organic transistor-type gas sensor and a zeolite with strong gas-adsorbing properties is proposed and experimentally demonstrated. Among the various investigated zeolites, ZSM-5 with ∼5.5 Å pore openings enhanced the adsorption for small gas molecules when combined with a polymer active layer, where it provided a pathway for gas molecules to penetrate the zeolite channels. Moreover, nitrided ZSM-5 (N-ZSM-5) enhanced the sensing performance of NO_2 molecules selectively because N in the N-ZSM-5 framework strongly interacted with NO_2 molecules. These results open the possibility for zeolite-modified organic gas sensors that selectively adsorb target gas molecules *via* heteroatoms substituted into the zeolite framework.

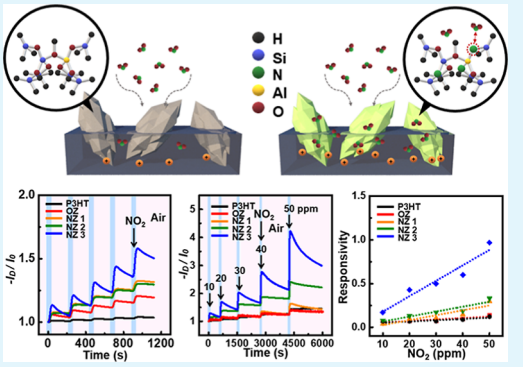

KEYWORDS: *nitridation, organic transistor, ZSM-5, P3HT, gas sensor*

1. INTRODUCTION

Air pollution has become a major environmental threat, and portable gas sensors, which can be used to detect harmful oxide gases such as NOx and SOx, have attracted attention from researchers.[1−5] For next-generation gas sensors, conductive polymers have strong potential for overcoming the existing deficiencies of conventional sensors based on inorganic metallic oxides. Organic semiconductors are expected to have excellent utility as portable soft devices because of their outstanding advantages, which include a low volumetric mass density, good flexibility, and compatibility with solution-based large-scale fabrication processes.[6−8] Because most organic semiconductors respond to polar gases such as NO_2 and SO_2, both high selectivity and good sensitivity are critical in an organic gas sensor. Despite the vast potential of organic semiconductors, their sensitivity and response rates, which affect the performance and reliability of organic gas sensors, are inadequate for them to be used in practical applications.[9−12] These weaknesses are closely associated with the thick organic active layer and intrinsically poor charge carrier characteristics of organic field-effect transistors (OFETs).[13−16]

An effective approach to improving the sensitivity and selectivity of organic gas sensors toward target gas molecules is to integrate organic semiconductors with functional materials for effective gas adsorption. Among such functional materials, zeolites are microporous aluminosilicate materials constructed from TO_4 (T = Si and Al) tetrahedra inter-bridged through O atoms. Zeolites are regarded as excellent adsorbents for harmful gas species because of their unique topological properties and adjustable composition *via* substitution of framework atoms, lattice O, and compensating cations.[17−19] In particular, modification of zeolites by tuning parts of their framework can expand their range of applications. Nitridation is a promising method to substitute lattice O with framework N, which has less electronegativity than O.[20] In our previous study, the most representative commercial zeolite, ZSM-5 (framework type MFI), showed excellent structural stability during nitridation at 900 °C.[21] In addition, a nitrided ZSM-5 (N-ZSM-5) film was explored for selective NO_2 adsorption depending on the compensating cations or Si/Al ratio.[22,23] With respect to this, N-ZSM-5 harbors robust potential as an outstanding analyte channel material for NOx gas sensors when it is blended with a conductive polymer as an active layer.

In the present study, we fabricated blend films based on a conductive polymer, poly(3-hexylthiophene) (P3HT), and ZSM-5 zeolites and characterized their performance as a sensitive and selective soft active layer in a gas sensor.[24] We expected the addition of zeolite to the polymer active layer to

Received: October 14, 2022
Accepted: January 17, 2023
Published: January 25, 2023

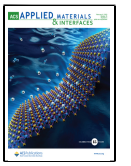

https://doi.org/10.1021/acsami.2c18498
ACS Appl. Mater. Interfaces 2023, 15, 7196−7203

improve gas adsorption because of the large specific surface area of the zeolite, which provides pathways for gas molecules to penetrate the channel region. In addition, we fabricated and compared a series of N-ZSM-5, in which some part of framework oxygen was substituted with nitrogen and the nitrogen content varied with the nitridation temperature. We modified N-ZSM-5 zeolites with different N contents and investigated the changes in their physicochemical properties when incorporated into blend films. In turn, the gas sensing properties of OFET-based sensors fabricated from P3HT/ZSM-5 blends were systematically investigated and compared to clarify the effects of the N content in ZSM-5 on the gas-sensing performance toward various gas molecules. OFETs can be used in sensitive portable sensors because of their functions with signal transducers and amplifiers.

2. EXPERIMENTAL SECTION

2.1. Nitridation of ZSM-5 Zeolites. A commercial aluminosilicate NH_4^+ form of ZSM-5 (SiO_2/Al_2O_3 = 23, CBV2314) used in the present study was purchased from Zeolyst. N-ZSM-5 was prepared *via* the previously reported procedures as mentioned in our report.[21] About 1.0 g of the NH_4-ZSM-5 sample was located in a tubular furnace and ramped to 500 °C with a heating rate of 2 °C min^{-1} under flowing N_2 (100 mL min^{-1}) and were kept at the equal condition for 2 h. After the shift into a flowing pure NH_3 (100 mL min^{-1}), the temperature was increased with a heating rate of 2 °C min^{-1} to 500, 700, or 900 °C to facilitate the N-ZSM-5 zeolites with diverse N amounts. After that, the furnace was maintianed at a particular temperature for 20 h under flowing NH_3 (100 mL min^{-1}) and then cooled naturally with pure N_2 (100 mL min^{-1}). Here, the three nitrided and the pristine NH_4-ZSM-5 zeolites are denoted as NZ 1 (500 °C), NZ 2 (700 °C), NZ 3 (900 °C), and OZ, respectively.

2.2. Characterization of ZSM-5 Zeolites. A Rigaku SmartLab X-ray diffractometer equipped with a Cu Kα radiation source was used to record powder X-ray diffraction (XRD) patterns in the 2θ range from 3 to 50° by scanning at a rate of 4° min^{-1}. N_2 sorption isotherms were collected using a Micromeritics Tristar II analyzer. Vario Micro CHNS was employed to measure the N content in the zeolite samples. The morphological properties of powders were determined using a Hitachi SU8010 scanning electron microscope operated with an accelerating voltage of 15 kV. X-ray photoelectron spectroscopy (XPS) spectra were measured on a PHI 5000 Versa Probe II equipped with an Al Kα radiation source ($h\nu$ = 1486.6 eV) using self-supporting zeolite wafers with a mass of ~20 mg and a diameter of 1.3 cm. The ^{29}Si MAS NMR spectra were collected on a 500 MHz Avance III HD Bruker solid-state NMR spectrometer at a spinning rate of 5 kHz, a ^{29}Si frequency of 99.36 MHz with a $\pi/2$ rad pulse length of 4 μs, a recycle delay of 60 s, and an acquisition of ~300 pulse transients. The Fourier transform infrared (FT-IR) spectra in the OH stretching region were obtained on a Nicolet 6700 FT-IR spectrometer using self-supporting zeolite wafers with a mass of ~12 mg and a diameter of 1.3 cm. Prior to the FT-IR measurements, pretreatment of the sample was performed under vacuum at 550 °C for 2 h inside a homemade IR cell with ZnSe windows.

2.3. Fabrication of the OFETs and Gas Sensors. P3HT (regioregularity = 95%, M_w = 58 kDa) was purchased from Rieke Metals. Various amounts of zeolites (10, 30, and 50 wt %) and 10 mg of P3HT were dissolved in 1 mL of chloroform. OFETs were fabricated on highly n-doped Si wafers as top-contact bottom-gate transistors. Si wafers with thermally grown 3000 Å-thick SiO_2 were washed sequentially in acetone and ethyl alcohol for 30 min in each solvent and then coated with hexamethyldisilazane (HMDS) using a spin-coating method at 2000 rpm for 30 s. The zeolite/P3HT blend films were fabricated on HMDS by spin-coating for 60 s at 2500 rpm. The source and drain electrodes were patterned onto the zeolite/P3HT blend films using a shadow mask (channel width = 2000 μm, channel length = 100 μm). For ultraviolet−visible (UV−vis) absorption analysis, the zeolite/P3HT blend films were spin-coated onto a coverglass subjected to identical surface treatments. After the fabrication process, the samples were kept under a high vacuum for 12 h.

2.4. Characterization of the OFETs and Gas Sensors. Optical microscopy (Olympus BX51) and field-emission scanning electron microscopy (JSM-7800F, JEOL) were used to characterize the morphologies and dispersion of zeolites in the P3HT films. The elemental mapping images of the blended films were investigated using the same instrument. UV−vis absorption spectra of blended films were recorded using a UV−vis spectrophotometer (PerkinElmer, Lambda 365). The electrical performance of the blend films was characterized under ambient conditions at RT (T_{avg} = 20.8 °C and relative humidity = 29%) using a semiconductor parametric analyzer (Keithley 4200). The field-effect mobility (μ) was determined in the saturation regime (V_D = −60 V) by plotting the I−V curves. The responses toward SO_2, CO_2, and NO_2 analytes were investigated using a gas sensor (Precision Sensor System, GASENTEST, Precision Sensor System) at a fixed gate voltage V_G of −10 V and a drain voltage V_D of −10 V. The target gas concentration was controlled by changing the mixing ratio of the target gas and air in a total gas flow rate of 500 mL min^{-1}.

3. RESULTS AND DISCUSSION

Figure 1a shows the powder XRD patterns of the OZ and NZ 1−3 zeolites. When compared with pristine OZ, all the nitrided

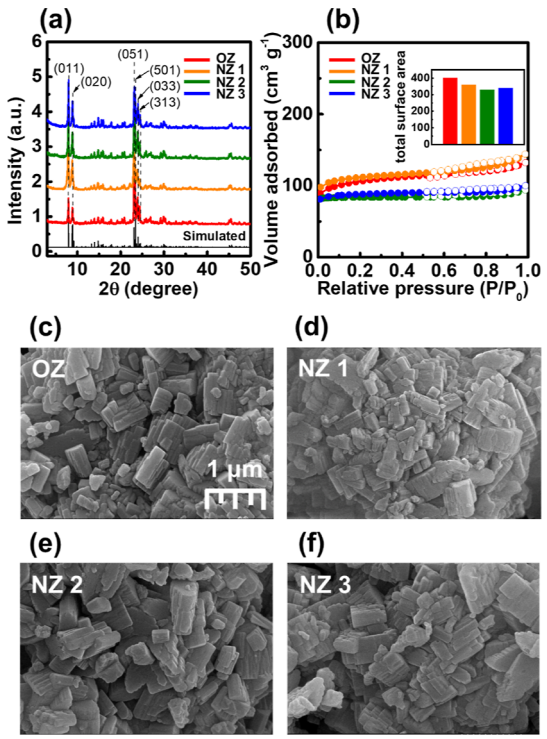

Figure 1. Representative characterization results that verify the topological properties of the samples employed in this study: (a) powder X-ray diffraction patterns, (b) N_2 sorption isotherms, and (c−f) scanning electron microscopy images of OZ and NZ 1−3.

NZ samples presented only characteristic MFI X-ray peaks at approximately 7.94, 8.80, 23.10, 23.42, 23.98, and 24.61°, corresponding to the (011), (020), (051), (501), (033), and (313) reflections, respectively.[25] The small full-width at half-maximum values of the peaks indicated that the samples were highly crystalline even after high-temperature nitridation. As shown in Figure 1b, all OZ and NZ samples exhibit the typical

https://doi.org/10.1021/acsami.2c18498
ACS Appl. Mater. Interfaces 2023, 15, 7196−7203

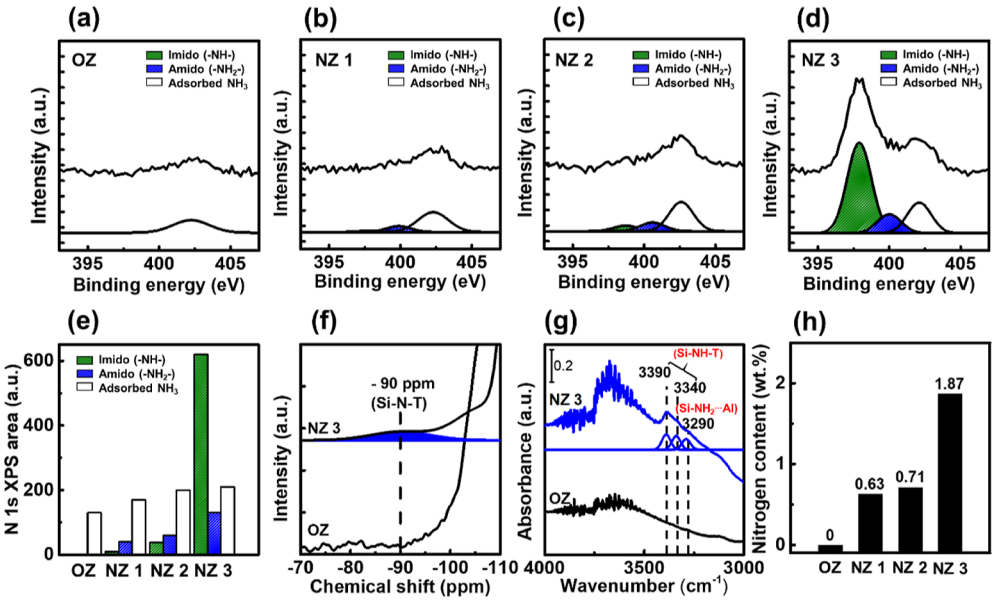

Figure 2. Representative characterization results verifying the substitution of N into the ZSM-5 framework during nitridation: (a–d) N 1s X-ray photoelectron spectroscopy spectra of OZ and NZ 1–3, (e) summary of N species revealed by deconvolution of the component N 1s spectra, (f) deconvoluted ^{29}Si MAS NMR spectra of OZ and NZ 3, (g) OH stretching region of the Fourier transform infrared spectra of OZ and NZ 3, and (h) CHN analysis results for OZ and NZ 1–3.

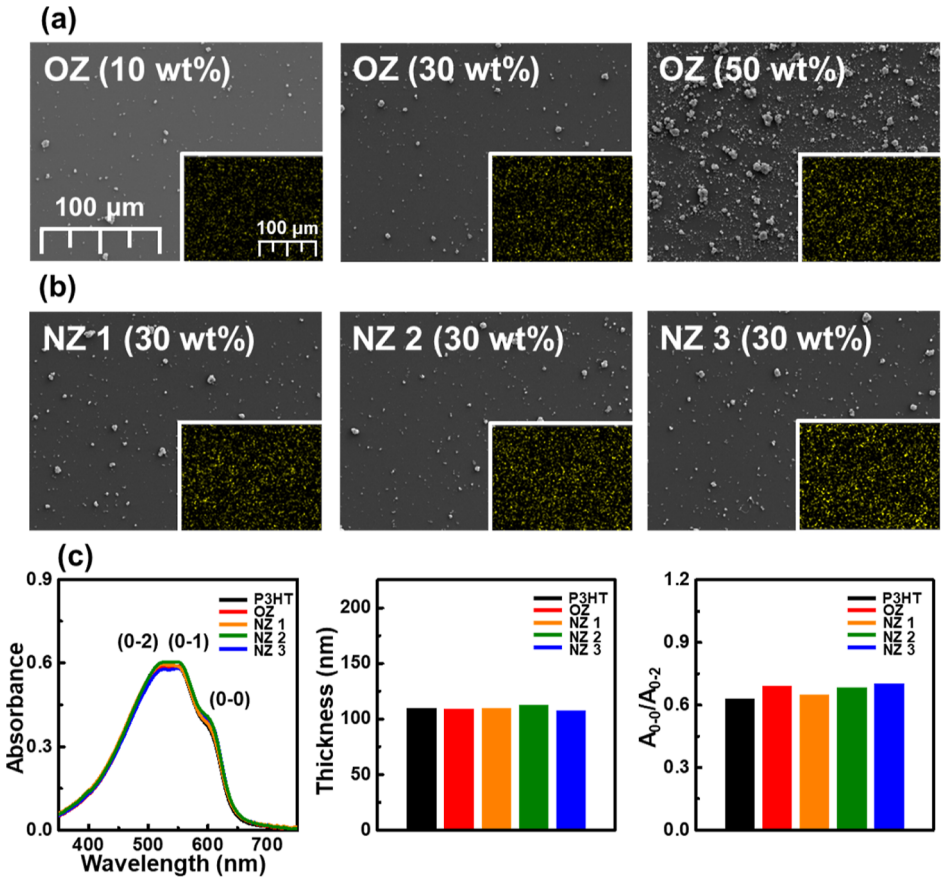

Figure 3. Scanning electron microscopy images of zeolite blend films (a) with various amounts of OZ and (b) with different types of nitrided zeolite. The inset shows the N elemental mapping images of the blend films. (c) UV–vis absorption spectra of P3HT films with 30 wt % of different zeolites, and the film thickness and the ratio of intensities of the (0–0) and (0–2) transitions of the P3HT films with 30 wt % of different zeolites.

type-I N_2 sorption isotherms without hysteresis loops, which imply the microporous materials, and the high total Brunauer–Emmett–Teller (BET) surface areas greater than 329 $m^2\ g^{-1}$. In addition, the micropore surface areas still remained, that is,

https://doi.org/10.1021/acsami.2c18498
ACS Appl. Mater. Interfaces 2023, 15, 7196–7203

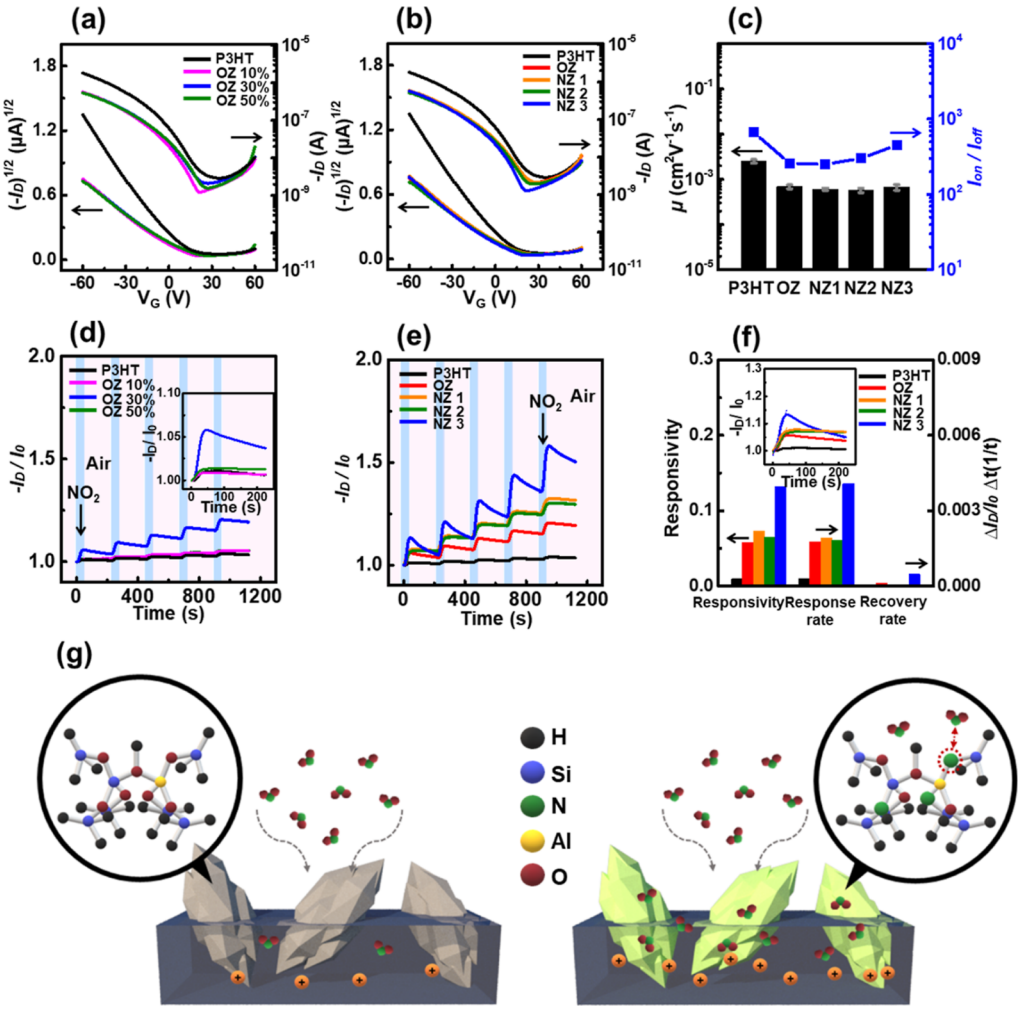

Figure 4. Electrical characteristics of organic field-effect transistors based on P3HT films containing (a) various amounts of OZ and (b) 30 wt % of different zeolites. (c) Charge carrier mobility and on−off ratio plots of a P3HT film and blended films. Responsivity plots of gas sensors based on blended films (d) with various amounts of OZ and (e) with 30 wt % of different zeolites. (f) Gas-sensing properties of the gas sensors based on P3HT/nitrided zeolite blended films. The inset shows the first cycle of the sensing curves. (g) Schematic of NO_2 gas adsorption of P3HT films blended with OZ and blended with NZ 3.

OZ = 292, NZ 1 = 283, NZ 2 = 315, and NZ 3 = 307 m^2 g^{-1} (Table S1). These results indicate the structural stability of zeolite samples with microporosity even after the high-temperature nitridation treatments at 500−900 °C. The scanning electron microscopy (SEM) images of OZ and NZ 1−3 (Figure 1c−f) show the same coffin shape with a similar submicron size (~570−700 nm), indicating that the morphology of NZ 1−3 did not change during the nitridation.

Figure 2a−d shows the N 1s XPS spectra of OZ and NZ 1−3 in the binding energy range of 393−407 eV. The bands at binding energies of >402, 398.1−400.1, and 397.7−398.5 eV are assigned to adsorbed NH_4^+ as a compensating cation within the zeolite channel, terminal amido species (−NH_2), and bridging imido species (−NH−), respectively.[24,26,27] The N 1s spectrum of the NH_4^+ form of pristine OZ showed only one band corresponding to the adsorbed NH_4^+ as compensating the cation electrically connected with the tetrahedral Al^{3+} atom in the zeolite framework. However, when ZSM-5 was nitrided at different temperatures, peaks assigned to terminal amido (−NH_2−) and bridging imido (−NH−) species intensified because of the reaction of N with silanol (≡Si−OH) groups and the substitution of N for O in the MFI framework, respectively (Figure 2e).[28] In particular, the XPS spectrum of NZ 3 showed an extremely intense peak for bridging imido (−NH−) species, indicating that the adsorbent contains stable N sites in its framework.

N-substitution into the ZSM-5 framework was further confirmed by ^{29}Si MAS NMR and FT-IR spectroscopies. As shown in Figure 2f, a weak but clear band at approximately −90 ppm was observed in the ^{29}Si MAS NMR spectrum of NZ 3 because of the existence of Si−N−T bonding.[29] The Si/Al ratios calculated from the ^{29}Si MAS NMR spectra of OZ and NZ 3 were 10.3 and 21.1, respectively, which means that partial dealumination occurred during the high-temperature (900 °C) treatment. As shown in Figure 2g, we observed the FT-IR bands corresponding to Si−NH−T and Si−NH_2···Al stretching vibrations at 3390, 3340, and 3290 cm^{-1},[30] which were not shown in the FT-IR spectrum of OZ. In addition, Figure 2h shows increasing N contents in NZ with increasing nitridation temperature, as determined by elemental analysis, consistent with the N 1s XPS results.

The surface morphology of the P3HT films with various amounts of the OZ and NZ 1−3 zeolites was characterized using SEM and energy-dispersive spectrometry (EDS)

https://doi.org/10.1021/acsami.2c18498
ACS Appl. Mater. Interfaces 2023, 15, 7196−7203

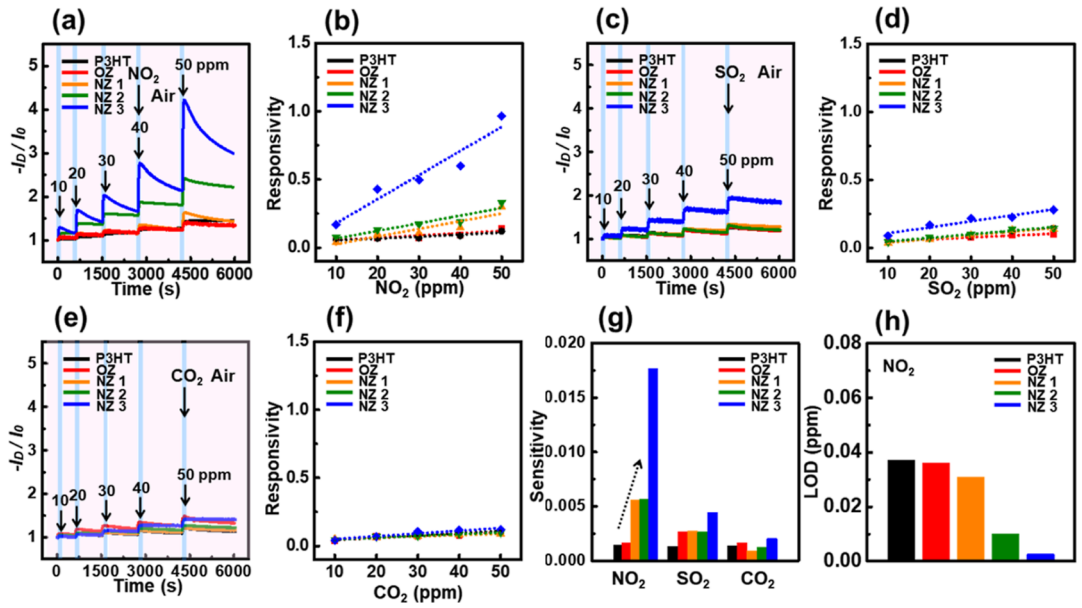

Figure 5. Gas sensing curve based on OFET gas sensors exposed to various concentrations of (a) NO_2, (c) SO_2, and (e) CO_2. The responsivity plots as a function of concentrations of (b) NO_2, (d) SO_2, and (f) CO_2 (insets show the sensitivity from the slope of the linear fitted graphs). (g) Sensitivity of gas sensors based on blended films when the sensors were exposed to various gases. (h) Calculated LOD values of fabricated gas sensors.

(Figures 3a,b and S1).[31−33] The SEM images confirmed that the zeolite particles were dispersed in the P3HT thin film. The P3HT film blended with 50 wt % of zeolite exhibited extensive aggregation of zeolites on the film surface. The EDS mapping images show that NZ 3, which was prepared at the highest nitridation temperature among the investigated samples, exhibited a higher N content in the P3HT films (Figure 3 inset). This result indicates that the nitridation temperature can be used to control the total N content in the blend films. We used UV−vis absorption spectra (Figure 3c) to evaluate the thicknesses and the changes in crystallinity of the P3HT films with various amounts of zeolite. The UV−vis spectra of P3HT films show similar absorption bands irrespective of the zeolite type.[34−37] The thicknesses and ratios of the (0−0) and (0−2) transitions of the P3HT films were calculated from their UV−vis spectra using the Beer−Lambert law. The Bee−Lambert law presents a relationship among the absorbance, molar extinction coefficient (ε), path length (l), and concentration (c): $A = \varepsilon lc$. The thickness values and A_{0-0}/A_{0-2} intensities of the P3HT films were similar to those of a homo-P3HT thin film. These results indicate that the zeolite type did not affect the thickness or molecular order in the P3HT films.

To evaluate the electrical performance of the P3HT/zeolite composite active layers, we fabricated OFETs with bottom-gate and top-contact devices on HMDS-treated SiO_2 substrates. P3HT films blended with zeolites showed a lower field-effect mobility value of 6.5×10^{-4} cm^2 V^{-1} s^{-1} compared with that of homo-P3HT films, which are almost equivalent values irrespective of the amounts and types of zeolites (Figures 4a−c and S2). The field-effect mobility and the on/off ratio were calculated from the I_D-V_G transfer curves of the OFETs.[38−45] The average field-effect mobility values and on-current levels were lower in the P3HT films with zeolite particles because the nonconducting ZSM-5 in the active layer interrupted the charge carrier transport. These results are consistent with those of previous studies involving the blending of conjugated polymers with nonconducting materials.[32,46,47]

We investigated the NO_2 gas-sensing performances of OFET gas sensors based on the P3HT/zeolite blend films with different degrees of nitridation.[48−53] The gas-sensing performances were measured in the linear region, at a fixed V_D of −10 V and a fixed V_G of −10 V. Figure 4d,e shows the changes in the normalized source−drain current $[I_D(t)/I_D(0)]$ when the fabricated gas sensors were repeatedly exposed to 10 ppm of NO_2 for 20 s and purged with air for 200 s. The P3HT film with 30 wt % of OZ exhibited the greatest increase in drain current compared to the homo-P3HT film and P3HT films with different amounts of OZ (Figures 4d and S3). The P3HT film with 50 wt % of OZ showed poor responsivity toward NO_2 gas, which indicates that the aggregation of zeolites interrupts the efficient approach of gas molecules toward the active layer. We blended 30 wt % of zeolites (i.e., the optimum amount of zeolites) into P3HT films and investigated the effect of the ZSM-5 N content on the NO_2 gas-sensing ability of the corresponding OFET sensors. Figure 4e shows that the OFET prepared using P3HT blended with NZ 3, which exhibited the highest N content, especially much higher concentration of stable imido (−NH−) species (Figure 2e), among the investigated samples, demonstrated the greatest improvement in responsivity compared with the responsivity of the device based on homo-P3HT. On the other hand, the OFET prepared using P3HT blended with NZ 1 and NZ 2 with relatively small N contents, especially much lower concentration of stable N species, showed the less improved responsivity compared to that of OZ. These results can be explained by the sensing performances of P3HT/ZSM-5 films for the target gas improving with increasing the concentration of stable N species in the ZSM-5 as a result of the strong interaction of the N atoms with NO_2 gas. In Figure 4f, the P3HT film with NZ 3 exhibited the greatest responsivity (defined as $R = \Delta I_D/I_{D0}$) as well as the highest response and recovery rates (defined as $\Delta R/\Delta t$). It is expected that if

https://doi.org/10.1021/acsami.2c18498
ACS Appl. Mater. Interfaces 2023, 15, 7196−7203

possible to increase the nitrogen content of nitrided zeolite more, it can result in further enhanced NO_2 gas sensing performance.

The gas-sensing mechanisms of the P3HT blend film are presented in the schematic in Figure 4g. Zeolites are well-known to function as gas adsorbents because of their microporous structure. In the case of ZSM-5, this structure provides a pathway for gas molecules to reach the active layer of the P3HT/ZSM-5 blend films. Moreover, NZ 3 exhibited the highest responsivity to NO_2, which confirms that N in the zeolite framework led to strong interaction with NO_2 molecules. Nitrogen in the imido groups exhibits electron-donating character; hence, N in N-ZSM-5 strongly interacts with NO_2 molecules. In addition, NO_2 is a strong electron acceptor that adsorbs electrons and generates holes in the active layer. When the P3HT/N-ZSM-5 blend film is exposed to NO_2 molecules, hole charge accumulation occurs, which affects the current in OFET-based gas sensors.[54]

We also characterized the gas-sensing properties of P3HT/ZSM-5 blend films for various gases at concentrations from 10 to 50 ppm (Figure 5). The OFET-based gas sensors showed an increase of the drain current with increasing the injection concentration of the analyte gases. The P3HT/ZSM-5 films demonstrated a stronger response toward NO_2 than toward SO_2 or CO_2. NO_2 gas has a strong electron-withdrawing character and generates more hole carriers than SO_2 or CO_2 in the P3HT film when the device is exposed to NO_2 gas. In particular, the sensitivity of P3HT/NZ 3 films toward NO_2 was notably higher than that toward the other gases in the order $NO_2 > SO_2 > CO_2$ (Figure 5g).[47] Calculated LOD values of fabricated gas sensors are summarized in Figure 5h. The LOD value of the P3HT film blended with NZ 3 was 0.0026 ppm, which is significantly lower than that of the homo-P3HT film and the previously reported LOD values (Table S2).[55−58] This result is related to the stronger interaction between N in the nitrided zeolite and NO_2 molecules compared with the interactions between N and the other gases, facilitating the selective detection of the target gas. The results presented here indicate that the nitridation of zeolite can be an effective approach to fabricating selectively sensitive organic gas sensors and that various functional groups will be useful for selectively sensing target gases.

4. CONCLUSIONS

We examined the potential of nitrided N-ZSM-5 zeolite as an analyte channel material inserted at the active layer in a gas sensor. N-ZSM-5 samples were prepared using three different nitridation temperatures to control the N content. Compared with a P3HT film without pristine ZSM-5, the ZSM-5/P3HT blend films showed substantially improved sensing properties, including enhanced responsivity, response rate, and recovery rate for various target gases. The microporous structure of the zeolite provided a pathway for gas molecules to penetrate the channel region. Moreover, N-ZSM-5 enhanced the sensing performance for NO_2 molecules selectively because N in N-ZSM-5 particles strongly interacted with NO_2 molecules. Our study demonstrated the usefulness of zeolites as a gas analyte channel in polymer gas-sensor applications and also demonstrated that the surface modification of zeolite has an excellent effect in selectively sensing target gases. We believe that the proposed method represents a new route for fabricating conjugated polymer/porous nanocomposite-based, high-performance gas sensors with high responsivity and good operational reliability.

ASSOCIATED CONTENT

Supporting Information

The Supporting Information is available free of charge at https://pubs.acs.org/doi/10.1021/acsami.2c18498.

BET specific surface areas of zeolite samples used in the present study; summary of LOD, response rate, and recovery rate of OFETs based on P3HT films; SEM images of thin films; electrical characteristics of OFETs based on P3HT films with various amounts of NZ 3; responsivity plots of gas sensors based on blended films with various amounts of NZ 3 (PDF)

AUTHOR INFORMATION

Corresponding Authors

Min Bum Park − *Department of Energy and Chemical Engineering, Incheon National University, Incheon 22012, Republic of Korea;* orcid.org/0000-0003-0788-1130; Email: mbpark@inu.ac.kr

Yeong Don Park − *Department of Energy and Chemical Engineering, Incheon National University, Incheon 22012, Republic of Korea;* orcid.org/0000-0002-1615-689X; Email: ydpark@inu.ac.kr

Authors

Yea Eun Hahm − *Department of Energy and Chemical Engineering, Incheon National University, Incheon 22012, Republic of Korea*

Sungjoon Kweon − *Department of Energy and Chemical Engineering, Incheon National University, Incheon 22012, Republic of Korea*

Complete contact information is available at: https://pubs.acs.org/10.1021/acsami.2c18498

Author Contributions

†Y.E.H. and S.K. contributed equally to this work.

Notes

The authors declare no competing financial interest.

ACKNOWLEDGMENTS

This work was supported by the National Research Foundation of Korea (NRF) grant funded by the Korea government (MSIT) (no. NRF-2021R1F1A149086) and the Basic Science Research Program through the National Research Foundation of Korea (NRF) funded by the Ministry of Science, ICT and Future Planning (2022R1F1A1065523).

REFERENCES

(1) Boningari, T.; Smirniotis, P. G. Impact of Nitrogen Oxides on the Environment and Human Health: Mn-Based Materials for the NOx Abatement. *Curr. Opin. Chem. Eng.* **2016**, *13*, 133−141.

(2) Anderson, J. O.; Thundiyil, J. G.; Stolbach, A. Clearing the Air: A Review of the Effects of Particulate Matter Air Pollution on Human Health. *J. Med. Toxicol.* **2012**, *8*, 166−175.

(3) Susanto, A. D. *Air Pollution and Human Health*, 2020, 10.13181/mji.com.204572.

(4) Bessac, B. F.; Jordt, S. E. Sensory Detection and Responses to Toxic Gases: Mechanisms, Health Effects, and Countermeasures. *Proc. Am. Thorac. Soc.* **2010**, *7*, 269−277.

(5) Munawer, M. E. Human Health and Environmental Impacts of Coal Combustion and Post-Combustion Wastes. *J. Sustain. Min.* **2018**, *17*, 87−96.
(6) Yu, S. H.; Girma, H. G.; Sim, K. M.; Yoon, S.; Park, J. M.; Kong, H.; Chung, D. S. Polymer-Based Flexible NO_x Sensors with ppb-Level Detection at Room Temperature using Breath-Figure Molding. *Nanoscale* **2019**, *11*, 17709−17717.
(7) Zhang, C.; Chen, P.; Hu, W. Organic Field-Effect Transistor-Based Gas Sensors. *Chem. Soc. Rev.* **2015**, *44*, 2087−2107.
(8) Das, A.; Dost, R.; Richardson, T. H.; Grell, M.; Wedge, D. C.; Kell, D. B.; Morrison, J. J.; Turner, M. L. Low Cost, Portable, Fast Multiparameter Data Acquisition System for Organic Transistor Odour sensors. *Sens. Actuators, B* **2009**, *137*, 586−591.
(9) Chen, H.; Dong, S.; Bai, M.; Cheng, N.; Wang, H.; Li, M.; Du, H.; Hu, S.; Yang, Y.; Yang, T.; Zhang, F.; Gu, L.; Meng, S.; Hou, S.; Guo, X. Solution-Processable, Low-Voltage, and High-Performance Monolayer Field-Effect Transistors with Aqueous Stability and High Sensitivity. *Adv. Mater.* **2015**, *27*, 2113−2120.
(10) Zhang, S.; Zhao, Y.; Du, X.; Chu, Y.; Zhang, S.; Huang, J. Gas Sensors Based on Nano/Microstructured Organic Field-Effect Transistors. *Small* **2019**, *15*, 1805196.
(11) Kang, B.; Jang, M.; Chung, Y.; Kim, H.; Kwak, S. K.; Oh, J. H.; Cho, K. Enhancing 2D Growth of Organic Semiconductor Thin Films with Macroporous Structures via a Small-Molecule Heterointerface. *Nat. Commun.* **2014**, *5*, 1−7.
(12) Nketia-Yawson, B.; Jung, A. R.; Noh, Y.; Ryu, G. S.; Tabi, G. D.; Lee, K. K.; Kim, B.; Noh, Y. Y. Highly Sensitive Flexible NH_3 Sensors Based on Printed Organic Transistors with Fluorinated Conjugated Polymers. *ACS Appl. Mater. Interfaces* **2017**, *9*, 7322−7330.
(13) Lee, Y. H.; Jang, M.; Lee, M. Y.; Kweon, O. Y.; Oh, J. H. Flexible Field-Effect Transistor-Type Sensors Based on Conjugated Molecules. *Chem* **2017**, *3*, 724−763.
(14) Li, H.; Shi, W.; Song, J.; Jang, H. J.; Dailey, J.; Yu, J.; Katz, H. E. Chemical and Biomolecule Sensing with Organic Field-Effect Transistors. *Chem. Rev.* **2019**, *119*, 3−35.
(15) Lee, M. Y.; Lee, H. R.; Park, C. H.; Han, S. G.; Oh, J. H. Organic Transistor-Based Chemical Sensors for Wearable Bioelectronics. *Acc. Chem. Res.* **2018**, *51*, 2829−2838.
(16) Ji, B.; Zhang, W. Adsorption of Cerium (III) by Zeolites Synthesized from Kaolinite after Rare Earth Elements (REEs) Recovery. *Chemosphere* **2022**, *303*, 134941.
(17) Cundy, C. S.; Cox, P. A. The Hydrothermal Synthesis of Zeolites: Precursors, Intermediates and Reaction Mechanism. *Microporous Mesoporous Mater.* **2005**, *82*, 1−78.
(18) Choi, S.; Drese, J. H.; Jones, C. W. Adsorbent Materials for Carbon Dioxide Capture from Large Anthropogenic Point Sources. *ChemSusChem* **2009**, *2*, 796−854.
(19) Morris, R. E.; Wheatley, P. S. Gas Storage in Nanoporous Materials. *Angew. Chem., Int. Ed.* **2008**, *47*, 4966−4981.
(20) Ernst, S.; Hartmann, M.; Sauerbeck, S.; Bongers, T. Novel Family of Solid Basic Catalysts Obtained by Nitridation of Crystalline Microporous Aluminosilicates and Aluminophosphates. *Appl. Catal., A* **2000**, *200*, 117−123.
(21) Kweon, S.; An, H.; Shin, C. H.; Park, M. B.; Min, H. K. Nitrided Ni/N-zeolites as Efficient Catalysts for the Dry Reforming of Methane. *J. CO_2 Util.* **2021**, *46*, 101478.
(22) Perdana, I.; Creaser, D.; Öhrman, O.; Hedlund, J. A Comparison of NOx Adsorption on Na, H and BaZSM-5 Films. *Appl. Catal., B* **2007**, *72*, 82−91.
(23) Mosca, A.; Öhrman, O.; Hedlund, J.; Perdana, I.; Creaser, D. NO_2 and N_2 Sorption in MFI Films with Varying Si/Al and Na/Al ratios. *Microporous Mesoporous Mater.* **2009**, *120*, 195−205.
(24) Min, H.-K.; Cha, S. H.; Hong, S. B. Nitrided ITQ-2 as an Efficient Knoevenagel Condensation Catalyst. *Chem. Commun.* **2013**, *49*, 1115−1117.
(25) Baerlocher, C.; McCusker, L. B. Database of Zeolite Structures. https://www.iza-structure.org/databases/ (accessed on December 01, 2022).
(26) Ederer, J.; Janoš, P.; Ecorchard, P.; Tolasz, J.; Štengl, V.; Beneš, H.; Perchacz, M.; Pop-Georgievski, O. Determination of Amino Groups on Functionalized Graphene Oxide for Polyurethane Nanomaterials: XPS Quantitation vs. Functional Speciation. *RSC Adv.* **2017**, *7*, 12464−12473.
(27) Srasra, M.; Delsarte, S.; Gaigneaux, E. M. Nitrided Zeolites: A Spectroscopic Approach for the Identification and Quantification of Incorporated Nitrogen Species. *J. Phys. Chem. C* **2010**, *114*, 4527−4535.
(28) Wu, G.; Wang, X.; Yang, Y.; Li, L.; Wang, G.; Guan, N. Confirmation of NH Species in the Framework of Nitrogen-Incorporated ZSM-5 Zeolite by Experimental and Theoretical Studies. *Microporous Mesoporous Mater.* **2010**, *127*, 25−31.
(29) Hammond, K. D.; Dogan, F.; Tompsett, G. A.; Agarwal, V.; Conner, W. C.; Grey, C. P.; Auerbach, S. M. Spectroscopic Signatures of Nitrogen-Substituted Zeolites. *J. Am. Chem. Soc.* **2008**, *130*, 14912−14913.
(30) Ernst, S.; Hartmann, M.; Hecht, T.; Cremades Jaén, P. C.; Sauerbeck, S. The Influence of Water on the Activity of Nitridated Zeolites in Base-Catalyzed Reactions. *Stud. Surf. Sci. Catal.* **2002**, *142*, 549−556.
(31) Saxena, V.; Aswal, D. K.; Kaur, M.; Koiry, S. P.; Gupta, S. K.; Yakhmi, J. V.; Kshirsagar, R. J.; Deshpande, S. K. Enhanced NO_2 Selectivity of Hybrid Poly(3-hexylthiophene): ZnO-Nanowire Thin Films. *Appl. Phys. Lett.* **2007**, *90*, 043516.
(32) Lee, J. I.; Kim, M.; Park, J. H.; Kang, B.; Lee, C. Y.; Park, Y. D. Metal-Organic Framework as a Functional Analyte Channel of Organic-Transistor-Based Air Pollution Sensors. *ACS Appl. Mater. Interfaces* **2021**, *13*, 24005−24012.
(33) Kwon, E. H.; An, H.; Park, M. B.; Kim, M.; Park, Y. D. Conjugated Polymer−Zeolite Hybrids for Robust Gas Sensors: Effect of Zeolite Surface Area on NO_2 Sensing Ability. *Chem. Eng. J.* **2021**, *420*, 129588.
(34) Hintz, H.; Egelhaaf, H. J.; Peisert, H.; Chassé, T. Photo-Oxidation and Ozonization of Poly(3-Hexylthiophene) Thin Films as Studied by UV/VIS and Photoelectron Spectroscopy. *Polym. Degrad. Stab.* **2010**, *95*, 818−825.
(35) Ehrenreich, P.; Birkhold, S. T.; Zimmermann, E.; Hu, H.; Kim, K. D.; Weickert, J.; Pfadler, T.; Schmidt-Mende, L. H-Aggregate Analysis of P3HT Thin Films-Capability and Limitation of Photoluminescence and UV/Vis Spectroscopy. *Sci. Rep.* **2016**, *6*, 1−8.
(36) Yu, S. H.; Hassan, S. Z.; Nam, G.-H.; An, S.; Kang, B.; Chung, D. S. Consideration of Azobenzene-Based Self-Assembled Monolayer Deposition Conditions for Maximizing Optoelectronic Switching Performances. *Chem. Mater.* **2021**, *33*, 5991−6002.
(37) Park, S. Y.; Kwon, E. H.; Park, Y. D. Effect of Localized UV Irradiation on the Crystallinity and Electrical Properties of Dip-Coated Polythiophene Thin Films. *RSC Adv.* **2020**, *10*, 34130−34136.
(38) Raveendran, R.; Namboothiry, M. A. G. Bias Stress Stability and Hysteresis in Elastomeric Dielectric Based Solution Processed OFETs. *Mater. Res. Bull.* **2022**, *146*, 111596.
(39) Torsi, L.; Dodabalapur, A.; Sabbatini, L.; Zambonin, P. G. Multi-Parameter Gas Sensors Based on Organic Thin-Film-Transistors. *Sens. Actuators, B* **2000**, *67*, 312−316.
(40) Chang, J. F.; Hou, K. S.; Yang, Y. W.; Wang, C. H.; Chen, Y. X.; Ke, H. Enhanced Mobility for Increasing On-Current and Switching Ratio of Vertical Organic Field-Effect Transistors by Surface Modification with Phosphonic Acid Self-Assembled Monolayer. *Org. Electron.* **2020**, *81*, 105689.
(41) Zhang, J.; Xu, J.; Lim, J.; Nolan, J. K.; Lee, H.; Lee, C. H. Wearable Glucose Monitoring and Implantable Drug Delivery Systems for Diabetes Management. *Adv. Healthcare Mater.* **2021**, *10*, No. e2100194.
(42) Hou, S.; Yu, J.; Zhuang, X.; Li, D.; Liu, Y.; Gao, Z.; Sun, T.; Wang, F.; Yu, X. Phase Separation of P_3HT/PMMA Blend Film for Forming Semiconducting and Dielectric Layers in Organic Thin-Film Transistors for High-Sensitivity NO_2 Detection. *ACS Appl. Mater. Interfaces* **2019**, *11*, 44521−44527.

https://doi.org/10.1021/acsami.2c18498
ACS Appl. Mater. Interfaces 2023, 15, 7196−7203

(43) Oh, S.; Khan, M. R. R.; Choi, G.; Seo, J.; Park, E.; An, T. K.; Park, Y. D.; Lee, H. S. Advanced Organic Transistor-Based Sensors Utilizing a Solvatochromic Medium with Twisted Intramolecular Charge-Transfer Behavior and Its Application to Ammonia Gas Detection. *ACS Appl. Mater. Interfaces* **2021**, *13*, 56385−56393.
(44) Di, C. A.; Zhang, F.; Zhu, D. Multi-Functional Integration of Organic Field-Effect Transistors (OFETs): Advances and Perspectives. *Adv. Mater.* **2013**, *25*, 313−330.
(45) Zang, Y.; Zhang, F.; Huang, D.; Di, C. A.; Meng, Q.; Gao, X.; Zhu, D. Specific and Reproducible Gas Sensors Utilizing Gas-Phase Chemical Reaction on Organic Transistors. *Adv. Mater.* **2014**, *26*, 2862−2867.
(46) Jang, Y. J.; Jung, Y. E.; Kim, G. W.; Lee, C. Y.; Park, Y. D. Metal-Organic Frameworks in a Blended Polythiophene Hybrid Film with Surface-Mediated Vertical Phase Separation for the Fabrication of a Humidity Sensor. *RSC Adv.* **2019**, *9*, 529−535.
(47) Kang, Y.; Kwak, D. H.; Kwon, J. E.; Kim, B. G.; Lee, W. H. NO_2-Affinitive Conjugated Polymer for Selective Sub-Parts-Per-Billion NO_2 Detection in a Field-Effect Transistor Sensor. *ACS Appl. Mater. Interfaces* **2021**, *13*, 31910−31918.
(48) Song, J.; Guo, T.; Huang, C.; Liu, M.; Cui, H.; Huang, W.; Wang, Y.; Li, T. Part per Trillion Level DMMP Gas Sensor Based on Calixarene Modified Organic Thin Film Transistor. *Chem. Eng. J.* **2022**, *446*, 137097.
(49) Cheon, H. J.; Shin, S. Y.; Tran, V.; Park, B.; Yoon, H.; Chang, M. Preparation of Conjugated Polymer/Reduced Graphene Oxide Nanocomposites for High-Performance Volatile Organic Compound Sensors. *Chem. Eng. J.* **2021**, *425*, 131424.
(50) Kumar, A.; Alami Mejjati, N.; Meunier-Prest, R.; Krystianiak, A.; Heintz, O.; Lesniewska, E.; Devillers, C. H.; Bouvet, M. Tuning of Interfacial Charge Transport in Polyporphine/Phthalocyanine Heterojunctions by Molecular Geometry Control for an Efficient Gas Sensor. *Chem. Eng. J.* **2022**, *429*, 132453.
(51) Mirza, M.; Wang, J.; Wang, L.; He, J.; Jiang, C. Response Enhancement Mechanism of NO_2 Gas Sensing in Ultrathin Pentacene Field-Effect Transistors. *Org. Electron.* **2015**, *24*, 96−100.
(52) Hahm, Y. E.; Park, B. H.; Park, S. Y.; An, T. K.; Lee, J.; Park, Y. D. Enhancement of NO_2 Gas Sensing Ability through Strong Binding Energy by Modification of Interface Characteristics. *Org. Electron.* **2022**, *104*, 106493.
(53) Oh, J.; Lee, J. S.; Jun, J.; Kim, S. G.; Jang, J. Ultrasensitive and Selective Organic FET-Type Nonenzymatic Dopamine Sensor Based on Platinum Nanoparticles-Decorated Reduced Graphene Oxide. *ACS Appl. Mater. Interfaces* **2017**, *9*, 39526−39533.
(54) Wei, S.; Tian, F.; Ge, F.; Wang, X.; Zhang, G.; Lu, H.; Yin, J.; Wu, Z.; Qiu, L. Helical Nanofibrils of Block Copolymer for High-Performance Ammonia Sensors. *ACS Appl. Mater. Interfaces* **2018**, *10*, 22504−22512.
(55) Han, S.; Yang, Z.; Li, Z.; Zhuang, X.; Akinwande, D.; Yu, J. Improved Room Temperature NO_2 Sensing Performance of Organic Field-Effect Transistor by Directly Blending a Hole-Transporting/Electron-Blocking Polymer into the Active Layer. *ACS Appl. Mater. Interfaces* **2018**, *10*, 38280−38286.
(56) Wagner, J.; Song, Y.; Shapiro, J.; Katz, H. E. Oxygen-Bearing Functionalities Enhancing NO_2, NH_3, and Acetone Electronic Response and Response Variation by Polythiophenes in Organic Field-Effect Transistor Sensors. *J. Mater. Chem. C* **2022**, *10*, 2149.
(57) Wagner, J.; Jang, H.-J.; Han, J.; Katz, H. E. Enhanced and Unconventional Responses in Chemiresistive Sensing Devices for Nitrogen Dioxide and Ammonia from Carboxylated Alkylthiophene Polymers. *Mater. Horiz.* **2020**, *7*, 1358.
(58) Peng, B. Y.; Huang, S. Y.; Zhou, Z. W.; Chan, P. K. L. Solution-Processed Monolayer Organic Crystals for High-Performance Field-Effect Transistors and Ultrasensitive Gas Sensors. *Adv. Funct. Mater.* **2017**, *27*, 1700999.

https://doi.org/10.1021/acsami.2c18498
ACS Appl. Mater. Interfaces 2023, 15, 7196−7203